International Journal of GEOMATE
(Geotechnique, Construction Materials and Environment)
ISSN: 2186-2982 (P), 2186-2990 (O), Japan

Vol. 31, Issue 143, July, 2026, pp.1-10; DOI: 10.21660/2026.143.5469

NONLINEAR BEHAVIOR AND IMPERFECTION SENSITIVITY OF HYBRID THREE-LAYER COMPOSITE BEAMS USING ENERGY-BASED MECHANISM ANALYSIS

Hong Son Nguyen[1], *Le Thuy Nguyen[2] and Thuy Van Tran Thi[3]

[1,2]Faculty of Civil Engineering, Hanoi Architectural University, Vietnam

*Corresponding Author, Received: 01 Feb. 2026, Revised: 24 Feb. 2026, Accepted: 10 Mar. 2026

ABSTRACT: This study investigates the nonlinear structural behavior and imperfection sensitivity of hybrid three-layer timber beams, which is a critical issue for slender composite members in modern timber engineering. Conventional linear beam theories are often inadequate to capture the second-order geometric effects arising under large transverse deflections. A geometrically nonlinear energy-based model is developed to describe the interaction between high-stiffness outer timber layers and a softer core material. The formulation explicitly accounts for initial geometric imperfections prescribed at the global beam level. A mechanism index, denoted as η, is introduced to quantify the relative contribution of membrane forces induced by large deflection to the overall structural response, thereby identifying the transition from bending-dominated to membrane-influenced behavior. Numerical simulations are conducted using MATLAB for beams with varying amplitudes of initial sinusoidal imperfection e_0. The results demonstrate that geometric imperfections significantly amplify membrane action, leading to an earlier onset of stiffness degradation compared with geometrically perfect beams. For relatively large imperfections, a reduction of tangent stiffness on the order of 40% is observed as the applied transverse load increases. Unlike conventional nonlinear beam studies primarily based on load–deflection comparison or full three-dimensional finite element simulations, the present work introduces an energy-based mechanism index (η) that quantitatively identifies nonlinear transition and enables derivation of serviceability-oriented knock-down factors for imperfection-sensitive composite timber beams.

Keywords: Hybrid timber beams, Nonlinear behavior, Membrane effect, Mechanism index, Imperfection sensitivity, Geometric nonlinearity

1. INTRODUCTION

Composite timber beams with partial interaction have been increasingly adopted in modern building and bridge structures owing to their favourable strength-to-weight ratio, sustainability, and adaptability for medium- and long-span applications. The structural behaviour of such members is governed by the interaction between bending deformation, interlayer slip, and bending-induced axial effects, which together determine stiffness, deflection, and overall serviceability performance [1–3]. To support practical design, simplified analytical approaches such as the γ-method have been widely used to estimate effective bending stiffness under linear-elastic assumptions [1,4].

However, for slender composite timber beams experiencing moderate-to-large transverse deflections, geometric nonlinearity becomes an essential aspect of the structural response. Second-order effects associated with curvature-induced axial strains may lead to the development of membrane forces, stiffness degradation, and nonlinear load–deflection behaviour that cannot be captured by linear or first-order analysis [4–6]. Recent numerical investigations published in [7,8] have highlighted the importance of accounting for such nonlinear deformation mechanisms in laminated and composite timber beams, even when the material behaviour remains elastic [9–11].

In practical applications, composite timber beams are rarely perfectly straight after fabrication and installation. Initial geometric imperfections may arise from material heterogeneity, manufacturing tolerances, moisture-induced deformation, long-term creep, and construction inaccuracies. Even relatively small initial curvature can significantly influence the nonlinear response by triggering second-order effects at early loading stages and amplifying sensitivity to geometric nonlinearity under transverse bending loads [6,12].

Within the framework of geometrically nonlinear beam theory, initial imperfections are known to modify the equilibrium path and to reduce effective stiffness by accelerating the development of bending-induced membrane forces. While imperfection sensitivity has been extensively investigated in the context of column stability, its

role in the large-deflection bending response of composite timber beams has received comparatively less systematic attention. Existing analytical and numerical studies often acknowledge the presence of initial imperfection, but typically assess its influence through direct comparison of load–deflection curves for selected imperfection amplitudes [4,5,13].

Although such studies provide valuable quantitative information, their interpretation is frequently limited to descriptive trends, such as increased deflection or reduced stiffness with increasing imperfection amplitude. The underlying mechanical mechanisms governing imperfection sensitivity- particularly the role of initial curvature as a trigger for membrane-force activation and stiffness degradation-are rarely examined explicitly. Moreover, different stiffness measures relevant to nonlinear response are often not clearly distinguished. Tangent stiffness, which governs incremental stability, and secant stiffness, which is closely related to serviceability performance, are frequently treated implicitly or interchangeably in the literature [6,14].

Although numerous studies have incorporated geometric nonlinearity and partial interaction into analytical and finite element frameworks, their interpretation is often limited to numerical load–deflection comparison or detailed three-dimensional simulations [15,16]. While such approaches provide accurate prediction, they do not explicitly quantify the mechanical transition from bending-dominated response to membrane-influenced behavior. As a result, designers lack a clear indicator identifying when geometric nonlinearity becomes structurally significant at the serviceability level.

In contrast, the present study introduces an energy-based mechanism index (η) that explicitly partitions bending and membrane energy contributions. This formulation enables quantitative identification of nonlinear transition and provides a rational basis for deriving knock-down factors applicable to imperfection-sensitive serviceability assessment.

The objective of the present study is to perform a mechanism-based analysis of imperfection-sensitive geometric nonlinearity in hybrid composite timber beams subjected to transverse bending. Using a nonlinear analytical–numerical framework, the study aims to identify the mechanical mechanisms governing membrane-force activation, stiffness degradation, and deformation evolution in the presence of initial geometric imperfection e_0.

2. RESEARCH SIGNIFICANCE

The significance of this research lies in establishing a mechanism-based quantitative framework for evaluating hybrid composite timber beams beyond conventional descriptive load–deflection analysis. The study introduces a mechanism index to identify transitions between bending-dominant and membrane-dominant behaviour, enabling improved understanding of nonlinear structural response. It further quantifies the influence of geometric imperfections on stiffness degradation and stability, providing explicit relationships relevant to structural safety assessment. By integrating interface slip effects and hybrid material interaction into a unified modelling approach, the research offers practical design-oriented insights, including stability sensitivity indicators and simplified knock-down factors. These contributions enhance the reliability and design applicability of slender hybrid timber structures under realistic conditions.

3. THEORETICAL FORMULATION

The geometrically nonlinear behavior of hybrid three-layer timber beams with partial interaction is formulated based on the principle of minimum total potential energy. The model accounts for the longitudinal stretching of the neutral axis, which becomes significant under moderate-to-large deflections exacerbated by initial geometric imperfections.

3.1. Structural Configuration and Discretization Model

The nonlinear analysis of the hybrid three-layer timber beam is based on a discretized energy formulation. As illustrated in Fig. 1, the specimen is modeled as a composite system where the high-stiffness Birch faces and the Pine core are treated as distinct layers integrated through an elastic shear interface.

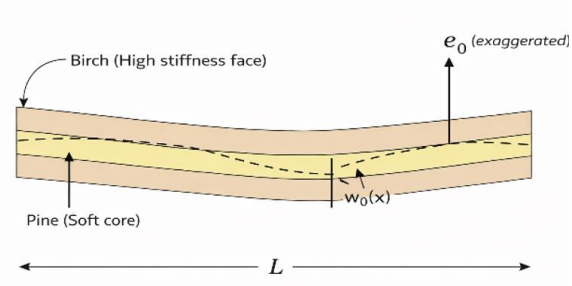

Fig. 1. Composite timber beam with initial geometric imperfection and interlayer slip

To facilitate the numerical solution, the structural domain is discretized into a series of nodes along the span L. This discretization model allows for the precise calculation of the following kinematic and geometric variables at each nodal point:

Global Imperfection $\omega_0(x)$: Defined at each node based on the sinusoidal function $\omega_0(x)=e_0.\sin(\pi x/L)$.

Layer-specific Displacements: The model tracks the longitudinal displacement u for each layer and a unified transverse deflection ω_a, accounting for the second-order effects induced by the imperfection.

Interlayer Slip (s): The relative movement between the Birch and Pine layers is evaluated at the interface nodes, governed by the slip stiffness k_s.

This discretized approach is essential for capturing the localized transition from bending to membrane action. By summing the potential energy contributions from each discrete element, the total energy functional Π is minimized to determine the nonlinear equilibrium path and the resulting stiffness degradation.

The beam is assumed to follow the Euler-Bernoulli hypothesis for individual layers, with an elastic interface allowing for interlayer slip. To capture geometric nonlinearity, the von Kármán strain-displacement relationship is employed. The total transverse displacement ω(x) is defined as the sum of the initial sinusoidal imperfection $\omega_0(x)$ and the additional deflection $\omega_a(x)$ induced by the load P [9, 10]:

$$\omega(x)=\omega_0(x)+\omega_a(x)=e_0\sin\frac{\pi x}{L}+\omega_a(x) \tag{1}$$

The longitudinal strain ε_x at the neutral axis of the composite section, considering the second-order effect of curvature, is given by [9, 12]:

$$\varepsilon_x=\frac{du}{dx}+\frac{1}{2}\left[\left(\frac{d\omega}{dx}\right)^2-\left(\frac{d\omega_0}{dx}\right)^2\right] \tag{2}$$

3.2. Energy Components

The total potential energy Π of the system is the summation of the internal strain energy and the potential of external loads [10]:

$$\Pi=U_b+U_m+U_s-\mathrm{W}_{ext} \tag{3}$$

Bending Energy U_b: Represents the energy due to curvature and effective flexural stiffness EI_{eff} [1, 4]:

$$U_b=\frac{1}{2}\int_0^L EI_{eff}\left(\frac{d^2\omega_a}{dx^2}\right)^2dx \tag{4}$$

Membrane Energy U_m: Represents the energy resulting from the induced axial tension (membrane force N_{mem} as the beam stretches [6].

$$U_m=\frac{1}{2}\int_0^L EA\varepsilon_x^2dx \tag{5}$$

Slip Energy U_s: Accounts for the work done by the shear flow against the elastic fasteners with stiffness k_s [2, 3].

$$U_s=\frac{1}{2}\int_0^L k_s\cdot s(x)^2dx \tag{6}$$

To further clarify the physical interpretation of the nonlinear response, the evolution of individual energy components during loading is examined. The results demonstrate progressive redistribution of energy from bending-dominated behavior toward membrane-influenced response as deflection increases. This energy evolution provides a direct mechanistic basis for interpreting the proposed mechanism index (η).

3.3. Mechanism Index η for Nonlinear Transition

To quantify the transition from bending-dominant to membrane-dominant behavior, a dimensionless mechanism index η is introduced:

$$\eta=\frac{U_m}{U_b+U_m} \tag{7}$$

This index is essential for identifying the transition load P*, defined as the load level where η reaches a critical threshold (typically η = 0.2), signifying that membrane effects are no longer negligible in the structural assessment.

3.4. Stiffness Degradation Measures

The nonlinear equilibrium path is characterized by two distinct stiffness measures:

- Tangent Stiffness K_{tan}: Defined by the second derivative of the potential energy $\frac{\partial^2\Pi}{\partial\omega_a^2}$, representing the instantaneous resistance to incremental loading.
- Secant Stiffness K_{sec}: Defined as P/ω_a, providing a global measure of structural efficiency relevant to serviceability limits.

Furthermore, the study rigorously distinguishes between tangent stiffness K_{tan} and secant stiffness K_{sec}. The tangent stiffness is a measure of the beam's instantaneous resistance to incremental changes in load, and its degradation rate is a vital indicator of impending structural instability. By analyzing the decay of K_{tan} relative to the imperfection magnitude e_0, we can establish knock-down factors that are essential for the safe design of hybrid timber structures under realistic engineering tolerances.

The schematic illustrates the hybrid

configuration consisting of high-stiffness Birch face layers and a soft Pine core. The initial geometric imperfection, denoted as $\omega_0(x)$ with amplitude e_0, is modeled as a global sinusoidal deviation of the beam's neutral axis rather than a localized defect within a single layer. This global curvature affects the entire composite cross-section and serves as the primary trigger for second-order geometric nonlinearities and membrane force activation. Note: The amplitude of the imperfection and the resulting deflections are exaggerated in the diagram to clearly visualize the kinematic interaction and interlayer slip distribution.

Composite timber beams with partial interaction exhibit a nonlinear response governed by the combined effects of bending deformation, interlayer slip, and axial deformation. In the present study, the composite action is represented at the member level using an equivalent stiffness idealization, which captures the global bending behaviour without resolving individual fasteners. This approach enables clear interpretation of governing response mechanisms while avoiding unnecessary modelling complexity.

Geometric nonlinearity is introduced through second-order kinematic relations, in which axial strain components associated with transverse displacement are explicitly considered. For slender beams subjected to moderate or large deflections, these nonlinear strain terms activate axial membrane forces that significantly influence stiffness characteristics and the nonlinear equilibrium path.

The beam is modelled using Euler–Bernoulli beam theory, as the present study focuses on imperfection-sensitive geometric nonlinearity in slender composite timber beams, for which bending–membrane interaction dominates the response while shear deformation effects remain secondary.

4. ENERGY-BASED NUMERICAL FRAMEWORK FOR IMPERFECTION-SENSITIVE NONLINEAR ANALYSIS

Based on Sections 3.1–3.4, a nonlinear finite-element model was implemented in MATLAB to analyse three-layer composite timber beams with partial shear interaction, explicit initial imperfections, and geometric nonlinearity. The beam is discretised into two-node Euler–Bernoulli elements (four DOFs per element) as illustrated in Fig. 2. Crucially, the initial curvature field $\omega_0(x)$ is prescribed and propagated through all computational stages. The Fig. 2 illustrated the discretization of the hybrid composite beam into two-node Euler–Bernoulli elements with associated degrees of freedom. Each node possesses transverse displacement w and rotation θ. The prescribed initial geometric imperfection $w_0(x)$ is introduced at the element level and consistently propagated throughout the nonlinear solution procedure.

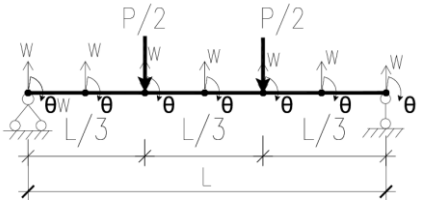

Fig. 2. Discretization of the three layer composite beam with degrees of freedom

4.1 Numerical Model and Reference Configuration

The following quantities are defined: span length L, width b, layer thickness t_1, t_2, material properties (E_1, A_1, I_1), (E_2, A_2, I_2); shear connection stiffness K_s, number of finite elements n_e, load increments n_{step}; initial imperfection $\omega_0(x)$

A geometrically nonlinear numerical model was developed in MATLAB to investigate the axial–flexural interaction and imperfection sensitivity of hybrid three-layer composite timber beams. The analysis focuses on the global structural response governed by large displacements and progressive membrane-force activation. The reference beam has a span length of L = 3.0 m and consists of three perfectly bonded layers with contrasting stiffness between the face layers and the core. An initial geometric imperfection is introduced at the member level and described by a sinusoidal function

$$\omega_0(x) = e_0 \cdot \sin\left(\frac{\pi x}{L}\right)$$

where e_0 denotes the imperfection amplitude at midspan.

The beam is discretized using two-node Euler–Bernoulli beam elements, and the axial load is applied incrementally. Unless otherwise stated, a sufficiently refined mesh is adopted to ensure numerical stability and mesh-independent results. Three imperfection ratios are considered in the study: δ_0/L = 1/600, 1/400, and 1/200.

4.2. Calculation of Interaction Coefficient and Effective Stiffness

Based on the material and connection characteristics, the composite interaction coefficient γ and the effective bending stiffness EI_{eff} are determined using the γ-method. These calculated parameters are then incorporated into the linear bending stiffness matrix $\mathbf{K_b}$, which serves as the basis for the subsequent nonlinear analysis.

4.3 Assembly of the Stiffness Matrix

For each element, the linear stiffness matrix $K_b^{(e)}$ is formulated and assembled into the global matrix [9]:

$$K_b = \sum_{e=1}^{n_e} K_b^{(e)} \tag{8}$$

Boundary conditions correspond to simple supports with zero overall axial extension:

$$\int_0^L u'(x)dx = 0 \tag{9}$$

The initial global displacement vector is set to:

$$\mathbf{U}_0=\{\omega_0, \theta_0, u_0\} \tag{10}$$

4.4. Incremental – Iterative Nonlinear Solution and Convergence Check

The numerical implementation was developed in MATLAB (version R2021b). The global nonlinear equilibrium equations are solved using a displacement-based finite element formulation with a direct linear solver at each Newton–Raphson iteration. Two-node Euler–Bernoulli beam elements with cubic interpolation for transverse displacement and linear interpolation for rotation are adopted. The global stiffness matrix is assembled following standard finite element conventions. Simply supported boundary conditions are enforced by prescribing zero transverse displacement at the supports, while overall longitudinal restraint is imposed by constraining the total axial deformation of the beam.

The external load is applied incrementally [9, 12]:

$$\mathbf{F}_{i+1}=\mathbf{F}_i + \mathbf{\Delta F} \tag{11}$$

At each load step, the current deflected shape ω(x) produces an axial membrane force:

$$N_{mem} = \frac{E_{eff} A_{eff}}{2L} \int_0^L \left(\theta(x)\right)^2 dx \tag{12}$$

Which contributes to the geometric stiffness matrix:

$$\mathbf{K}_g= \mathbf{N}_{mem}\cdot\mathbf{K}_g^* \tag{13}$$

The tangent stiffness is:

$$\mathbf{K}_t= \mathbf{K}_b+ \mathbf{K}_g \tag{14}$$

The incremental equilibrium equation is solved through Newton-Raphson iterations:

$$\mathbf{K}_t\mathbf{\Delta U}= \mathbf{\Delta F} \tag{15}$$

At the end of each iteration, the displacement vector **{U}** is updated, and the displacement error **‖ΔU‖** is checked against the convergence criterion. If the error remains above the tolerance, the load increment is reduced or additional Newton–Raphson iterations are performed for the current load step. The analysis proceeds iteratively until the specified load level or deflection limit is achieved.

Convergence is achieved when:

$$||\mathbf{\Delta U}|| < \varepsilon_{tol} \tag{16}$$

The load increment ΔF was prescribed as a fixed fraction of the estimated linear elastic reference load and was automatically reduced when convergence difficulties were encountered, particularly in the vicinity of rapid tangent stiffness degradation. In such cases, the load step size was decreased to improve numerical stability. A maximum number of 30 Newton–Raphson iterations was allowed per load step. The convergence tolerance ε_tol was set to 10^{-6} based on the Euclidean norm of the incremental displacement vector.

In the following numerical formulation, the applied transverse load is denoted by P at the structural level, while F represents the corresponding global force vector used in the finite element implementation.

Table 1. Nonlinear solution parameters used in the numerical analysis

Parameter name	Value
Initial increment ΔF	2-5% reference load
Convergence tolerance ε_{tol}	$1\cdot10^{-6}$
Maximum iteration per step	30
Step reduction factor	0.5

4.5. Output and Post Processing

After the analysis is completed, the program automatically produces graphical outputs, including the load–deflection (**P–δ**) curves for both perfect and imperfect beams, the distribution of axial forces ($\mathbf{N_{mem}}$), the tangent stiffness ($\mathbf{K_t(P)}$). It also provides comparisons between linear, geometrically nonlinear, and imperfect configurations, as well as parametric maps illustrating the influence of K_s L, and δ_0.

These results enable a systematic evaluation of how initial imperfections interact with shear connection stiffness and geometric nonlinearity.

A mesh convergence study was performed using 10, 20, 40, and 80 Euler–Bernoulli beam elements for representative loading and imperfection cases. The midspan deflection, membrane force, and tangent stiffness showed stable convergence as the mesh was refined, with differences below 1% beyond 40 elements. Based on this assessment, a discretization of 40 elements was adopted for all subsequent parametric analyses to ensure an appropriate balance between numerical accuracy and computational efficiency.

All numerical parameters, assumptions, and solution procedures are explicitly stated to facilitate reproducibility of the results.

5. NUMERICAL EXAMPLE

5.1 Input Data

To demonstrate the computational procedure and evaluate the influence of initial imperfections, a three-layer composite timber beam with partial shear connection is analyzed under symmetric four-point bending. The configuration corresponds to a simply supported beam subjected to two equal concentrated loads, a setup commonly employed in experimental studies to verify bending stiffness and nonlinear response.

The analysis is performed for a three-layer glued laminated timber beam connected by an elastic shear layer, modeled according to the γ-method described in Eurocode 5, Annex B. In addition to geometric nonlinearity (P–Δ effect), an explicit initial curvature $\omega_0(x)$ is introduced to simulate the natural out-of-straightness of the beam prior to loading. This imperfection serves as the trigger for second-order effects and enables evaluation of post-yield stiffness degradation and deflection amplification (see Fig. 4).

Geometric and material parameters: span L=3000mm; bottom layer width b_1=60mm and thickness t_1=15mm; core layer width b_2=60mm and thickness t_2=25mm; top layer width b_3=60mm and thickness t_3=15mm (identical to the bottom layer); elastic modulus $E_1=E_2=E_3$=11,000 MPa; connection shear stiffness K_s=600 N/mm.

The initial imperfection shape is defined as $\omega_0(x) = \delta_0 \cdot \sin\left(\frac{\pi x}{L}\right)$ with ratios δ_0/L=1/600, 1/400 and 1/200.

The initial imperfection $\omega_0(x)$ represents the unavoidable out-of-straightness of real beams. Expressing it as a function of x allows the nonlinear analysis to capture the actual curvature distribution along the span, which directly influences membrane-force generation and the P–Δ response.

The beam is discretized into 40 two-node Euler–Bernoulli finite elements (four degrees of freedom per element). The analysis is conducted incrementally until the target load or convergence criterion is reached, enabling comparison among perfect, geometrically nonlinear, and imperfect configurations. Analysis: The computations are carried out in MATLAB using finite-element code developed for three-layer composite timber beams. Three cases are analyzed and compared: Linear elastic analysis, without geometric nonlinearity or imperfections; Geometrically nonlinear analysis, including self-induced membrane forces (P–Δ effect); Imperfect beam analysis, accounting for prescribed initial curvature $\omega_0(x)$ with ratios δ_0/L=1/600, 1/400, 1/200.

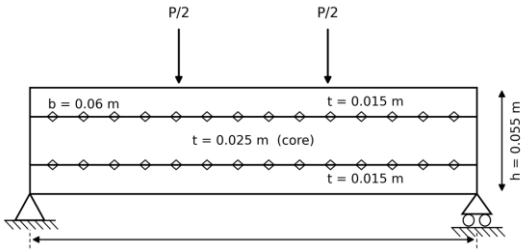

Fig. 3 Geometry and loading configuration of the imperfect composite beam

The effective bending stiffness EI_{eff} is evaluated using the γ-method according to Eurocode 5, Annex B, and assigned to the element stiffness matrices. The global tangent stiffness matrix is updated iteratively through the Newton–Raphson procedure until convergence is achieved at each load step. Initial imperfections are directly introduced into the displacement field before the first iteration, allowing the model to capture their influence on curvature, membrane-force generation, and the overall P–Δ response.

In the small-deflection range, the numerical results obtained from the present MATLAB implementation were verified against the analytical predictions of the γ-method specified in EN 1995-1-1. Excellent agreement was observed between the linear elastic load–deflection response and the γ-method solution, confirming that the formulation correctly reproduces the expected behavior before geometric nonlinearity and imperfection effects become significant.

In addition to the typical imperfection levels δ_o/L = 1/600 and 1/400, an upper-bound value of δ_o/L = 1/200 is considered to explore the sensitivity of the nonlinear response under severe but still plausible out-of-straightness conditions. This case is included to illustrate the limiting behavior of imperfection-sensitive stiffness degradation.

5.2 Results and Discussions

5.2.1. Influence of initial imperfection on global load-deflection behavior

The load–deflection responses in Figs. 4 and 5 demonstrate that initial imperfection leads to an early divergence from the linear reference response and amplifies the nonlinear softening of the beam. Even at small imperfection levels (δ_o/L = 1/600), the peak load and corresponding deflection are noticeably reduced, while larger imperfections (δ_o/L

= 1/200) cause a pronounced shift of the entire curve downward. This behavior reflects the combined action of geometric nonlinearity and the P–Δ effect, which magnifies the curvature induced by the initial out-of-straightness.

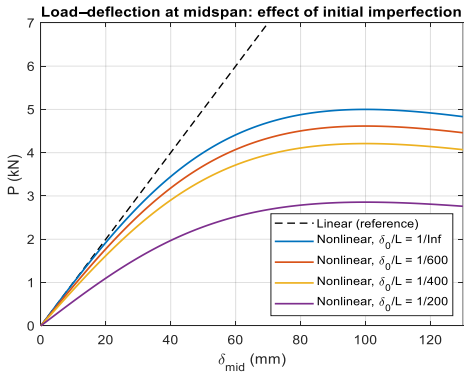

Fig. 4 Comparison of linear and nonlinear load–deflection curves under various imperfection ratios

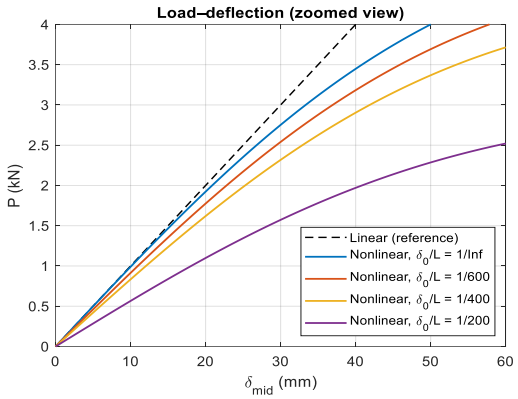

Fig. 5 Zoomed view of the initial P–δ response for various imperfection ratios (detail of Figure 4)

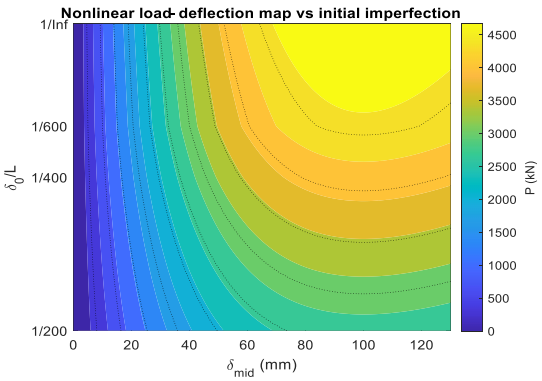

Fig. 6 Parametric contour plot of nonlinear load–midspan deflection response for different imperfection ratios

Figure 6 further generalizes this observation by presenting a two-dimensional response surface across a range of imperfections and mid-span deflections. The contour distribution shows that the region of maximum load gradually migrates toward smaller deflections as δ_o/L increases, indicating a reduction in both stiffness and ultimate resistance. The progressively compressed contour lines in the high-deflection zone highlight the increasing dominance of second-order effects, especially for larger imperfections. Overall, these results confirm that imperfection acts as a governing parameter that modifies not only the strength but the entire nonlinear response landscape of the beam.

5.2.2. Tangent and secant stiffness degradation under increasing deflection

Quantitatively, the reduction of stiffness exhibits a clear dependence on the imperfection ratio. For δ_o/L = 1/600, the tangent stiffness decreases by approximately 10–15% relative to the perfect-geometry case within the serviceability deflection range, while the corresponding secant stiffness reduction remains below about 10%. For δ_o/L = 1/400, the tangent stiffness reduction increases to roughly 20–30%, accompanied by a secant stiffness reduction of about 15–25%. In the upper-bound imperfection case δ_o/L = 1/200, the tangent stiffness approaches zero at moderate deflection levels, and the effective secant stiffness at serviceability may be reduced by up to approximately 40%.

The results further indicate that the deflection level at which the tangent stiffness approaches zero strongly depends on the imperfection amplitude. For small imperfections ($\delta_o/L \leq$ 1/600), the tangent stiffness remains positive throughout the investigated serviceability range. For δ_o/L = 1/400, the tangent stiffness approaches zero only at large deflections beyond typical serviceability limits. In contrast, for δ_o/L = 1/200, the tangent stiffness reaches near-zero values at relatively moderate deflections, indicating a pronounced imperfection sensitivity and an early onset of instability-prone behavior.

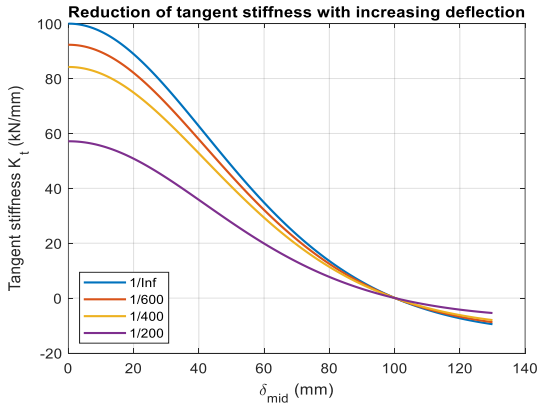

Fig. 7 Tangent stiffness K_t–midspan deflection curves for different initial imperfection amplitudes under

nonlinear analysis

The tangent stiffness curves in Fig. 7 reveal a rapid decline during the initial nonlinear stage, followed by a gradual softening as the deflection increases. Imperfection shifts the curves downward and promotes earlier stiffness reduction, especially for $\delta_o/L = 1/200$. This implies that beams with larger imperfections enter the instability-prone regime more quickly, where the tangent stiffness approaches zero or even becomes negative. Such behavior is characteristic of geometrically nonlinear members with curvature-induced bending amplification.

Meanwhile, the secant stiffness curves in Fig. 8 show a more uniform and monotonic reduction across the full range of deflection. Unlike the tangent stiffness, the shape of the secant degradation remains nearly parallel for all imperfection levels, suggesting that the global flexibility is primarily governed by the combined effect of bending deformation and accumulated curvature rather than by instantaneous stiffness changes. This distinction indicates that tangent stiffness governs stability phenomena, while secant stiffness better reflects the overall structural flexibility and service performance.

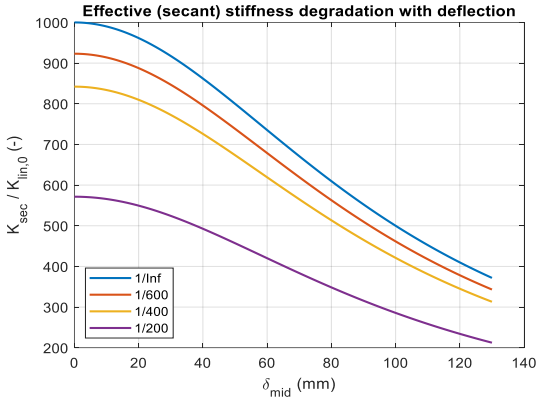

Fig. 8 Normalized secant stiffness $K_{sec}/K_{lin,0}$ as a function of midspan deflection for various imperfection ratios

The comparison of Figs. 7 and 8 highlights the complementary nature of tangent and secant measures: tangent stiffness is highly sensitive to imperfection and governs equilibrium path behavior, whereas secant stiffness provides more robust insight into long-span deflection and serviceability performance.

This duality underlines the importance of using both stiffness measures when evaluating slender timber or composite beams influenced by geometric nonlinearity.

The occurrence of zero or locally negative tangent stiffness reflects a loss of incremental stiffness due to imperfection-sensitive geometric nonlinearity, rather than numerical instability. Physically, it indicates a flattening or reversal of the equilibrium path and provides insight into the proximity of instability, not actual failure.

5.2.3. Serviceability performance and sensitivity of SLS stiffness to imperfection

The heat map in Fig. 9 shows that the effective stiffness at serviceability ($K_{sec}/K_{lin,0}$) is strongly influenced by both the imperfection ratio and the chosen deflection limit. Imperfections as small as $\delta_o/L = 1/600$ already cause a noticeable stiffness penalty, while $\delta_o/L = 1/200$ may reduce the service stiffness by more than 40%. This highlights those imperfections often considered minor in design can dominate the service behavior of slender beams.

Another key observation is that higher SLS limits (e.g., L/300) are more sensitive to imperfection effects, as reflected by the steeper gradient across the heat map. This suggests that systems designed with more permissive deflection limits may inadvertently experience disproportionate reductions in effective stiffness when imperfections are present. Conversely, stricter SLS limits (L/600) appear to mitigate some of this sensitivity because the evaluated deflections lie closer to the initial linear range.

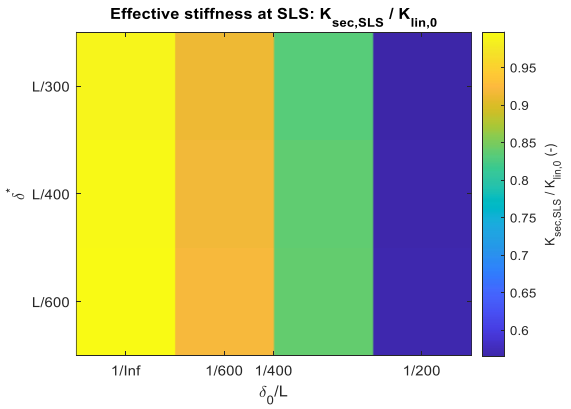

Fig. 9 Contour map of normalized secant stiffness $K_{sec}/K_{lin,0}$ at different midspan deflection levels and initial imperfection ratios

Figure 9 therefore emphasizes that the interaction between imperfection and service deflection limits must be considered explicitly in design. The smooth transition from high-stiffness (yellow) to low-stiffness (blue) regions illustrates the continuous manner in which imperfection affects SLS performance, rather than producing abrupt or threshold-based changes.

These findings underline the need for serviceability calculations that incorporate geometric imperfections, particularly in modern timber, steel, and composite structures with low inherent stiffness.

Notes:

The nonlinear trends obtained in this study are consistent with previously reported numerical and experimental results for partially composite timber beams [17]. The early reduction of tangent stiffness agrees with stiffness degradation trends observed in mechanically jointed timber members and composite beams with elastic shear connections [5,6,18]. The strong sensitivity of the nonlinear response to initial imperfection amplitude, illustrated in Figs. 4–9, also aligns with earlier findings showing that initial curvature accelerates membrane-force development and reduces effective stiffness at early loading stages [4,11,12]. Furthermore, the predicted reduction of effective bending stiffness at serviceability limit state falls within the range estimated by the γ-method in Eurocode 5 and subsequent studies on composite timber members [1,4]. The nonlinear load–deflection behaviour and contour response surfaces show good agreement with finite element predictions reported in previous studies [3,7,19–21].

Overall, these comparisons confirm that the proposed numerical framework captures the essential mechanisms governing geometric nonlinearity, partial interaction, and imperfection sensitivity in composite timber beams. However, the study is based on simplifying assumptions, including linear elastic material behaviour, idealized sinusoidal imperfections, and member-level modelling. Consequently, the derived knock-down factors and mechanism-based interpretations are primarily applicable to slender composite beams where geometric nonlinearity dominates prior to material failure. Application to cases involving significant material degradation, nonlinear connector behaviour, or complex three-dimensional boundary conditions should be undertaken with caution. From a design perspective, the mechanism index (η) may serve as an indicator of geometric nonlinearity at serviceability limits, with stiffness reduction recommended when η exceeds approximately 0.2.

6. CONCLUSIONS

This study investigated the influence of explicit initial geometric imperfections on the geometrically nonlinear behavior of three-layer composite timber beams with partial interaction. A numerical framework combining the γ-method, von Kármán geometric nonlinearity, and prescribed initial curvature was developed to capture membrane-force development and stiffness degradation.

The results demonstrate that initial imperfections significantly amplify deflection and accelerate tangent stiffness degradation, even at serviceability-level deformations. Compared with initially perfect beams, moderate imperfection amplitudes can lead to noticeable reductions in effective secant stiffness, highlighting a pronounced imperfection sensitivity that is not captured by conventional linear or perfect-geometry analyses.

From an engineering standpoint, the results highlight the importance of explicitly accounting for initial geometric imperfections when evaluating serviceability performance and stability behaviour of slender composite timber beams with partial interaction. The proposed MATLAB-based framework offers a transparent and computationally efficient approach for conducting imperfection-sensitive nonlinear analysis, supporting more informed performance-based design decisions.

The applicability of the present study is limited to the investigated parameter range, namely slender members with linear elastic material response and prescribed imperfection profiles. Although the proposed framework provides clear mechanistic insight and practical interpretation, further research is required to extend the approach to scenarios involving material nonlinearities or long-term effects such as creep.

7. REFERENCES

1. EN 1995-1-1: Eurocode 5 – Design of Timber Structures – Part 1-1: General – Common Rules and Rules for Buildings, CEN, Brussels, 2004, pp. 1–123.
2. A. Kroflič, I. Planinc, M. Saje, G. Turk, B. Čas, “Non-linear analysis of two-layer timber beams considering interlayer slip and uplift”, Engineering Structures, 32(6), 2010, pp. 1617–1630. https://doi.org/10.1016/j.engstruct.2010.02.009
3. J. Turmo, J.A. Lozano-Galant, E. Mirambell, D. Xu, “Modeling composite beams with partial interaction”, Journal of Constructional Steel Research, 114, 2015, pp. 380–393. https://doi.org/10.1016/j.jcsr.2015.07.007
4. L.T. Nguyen, H.S. Nguyen, T.V. Tran, “Geometric nonlinear analysis of two-layer timber composite beams with elastic connections using the γ-method in MATLAB”, International Journal of GEOMATE, 30(140), 2026, pp. 35–43. https://doi.org/10.21660/2026.140.5324
5. M.R. Salari, E. Spacone, P.B. Shing, D.M.

Frangopol, “Nonlinear analysis of composite beams with deformable shear connectors”, Journal of Structural Engineering, 124(10), 1998, pp. 1148–1158. DOI: 10.1061/(ASCE)0733-9445(1998)124:10(1148)
6. R.I.M. Al-Amery, T.M. Roberts, “Nonlinear finite difference analysis of composite beams with partial interaction”, Computers and Structures, 35(1), 1990, pp. 81–87. https://doi.org/10.1016/0045-7949(90)90258-4
7. T. Biliński, T. Socha, “Numerical analysis of deflections of multi-layered beams”, Civil and Environmental Engineering Reports, 15(4), 2014, pp. 33–42. https://doi.org/10.1515/ceer-2014-0033
8. M. Chybiński, A. Derlatka, P. Szewczyk et al., “Numerical investigation of steel-timber composite beams with cold-formed omega girders”, Archives of Civil Engineering, 71(3), 2025, pp. 523–537. DOI: https://doi.org/10.24425/ace.2025.155116
9. M.A. Crisfield, “Non-linear Finite Element Analysis of Solids and Structures”, Wiley, 1991, pp. 1–345.
10. J.N. Reddy, “Energy Principles and Variational Methods in Structural Mechanics”, Springer, 2017.
11. A.A. Shabana, “Geometric nonlinearity in beam-type structures”, Nonlinear Dynamics, 95, 2019.
12. J.M. Battini, C. Pacoste, “Co-rotational beam elements with warping effects in instability problems”, Computer Methods in Applied Mechanics and Engineering, 191, 2002, pp. 1755–1789. https://doi.org/10.1016/S0045-7825(01)00352-8
13. Y. De Santis, M. Fragiacomo, “Slip modulus formulas for timber-to-timber inclined screw connections – Comparison with other simplified models”, INTER Conference Paper, Paper No. 54-7-4, pp. 1–14.
14. N. Khorsandnia, H. Valipour, K. Crews, “Comparative study of analytical modelling of short- and long-term behaviour in timber-concrete composite systems”, World Conference on Timber Engineering, Auckland, New Zealand, 2012, pp. 304–312.
15. P. Ansourian, “Behaviour of stiffened composite beams with partial shear interaction accounting for time effects”, Procedia Engineering, 14, 2011, pp. 402–409. https://doi.org/10.1016/j.proeng.2011.07.050
16. S. Piriyasurawong, T. Techakitlachorn, “Finite element analysis of beam using 2×4 glued bamboo laminated with para timber and 2×6 para timber”, International Journal of GEOMATE, 20(80), 2021, pp. 182–187.
17. J. Barbalić, B. Zadravec, N. Perković, V. Rajčić, “Experimental study of timber composite beam elements using hardwood mechanically inserted and welded dowels”, Forests, 16, 2025, Article 1748. https://doi.org/10.3390/f16111748
18. P. Supe, J. Iejavs, “Bending properties of mechanically jointed solid timber beams”, Drewno, 60(199), 2017, pp. 151–159. https://doi.org/10.12841/wood.1644-3985.152.11
19. N. Khorsandnia, H. Valipour, K. Crews, “Structural response of timber-concrete composite beams predicted by finite element models and manual calculations”, Advances in Structural Engineering, 17(11), 2014, pp. 1601–1615. https://doi.org/10.1260/1369-4332.17.11.1601
20. M. Fragiacomo, “A finite element model for long-term analysis of timber-concrete composite beams”, Structural Engineering and Mechanics, 20(2), 2005, pp. 173–189. https://doi.org/10.12989/sem.2005.20.2.173
21. N. Khorsandnia, H. Valipour, K. Crews, “Finite element modeling of timber-concrete composite beams under short-term loadings”, ECCOMAS 2012 – European Congress on Computational Methods in Applied Sciences and Engineering, Vienna, Austria, 2012, pp. 1–9.

Copyright © Int. J. of GEOMATE All rights reserved, including making copies, unless permission is obtained from the copyright proprietors.